

Role of Nematic Fluctuations on Superconductivity in $\text{FeSe}_{0.47}\text{Te}_{0.53}$ Revealed by NMR under Pressure

Qing-Ping Ding,¹ Juan Schmidt,^{1,2} Jose A. Moreno,^{1,3} Sergey L. Bud'ko,^{1,2} Paul C. Canfield,^{1,2} and Yuji Furukawa^{1,2}

¹*Ames National Laboratory, U.S.DOE, Ames, Iowa 50011, USA*

²*Department of Physics and Astronomy, Iowa State University, Ames, Iowa 50011, USA*

³*Departamento de Física de la Materia Condensada,*

*Instituto Nicolás Cabrera and Condensed Matter Physics Center,
Universidad Autónoma de Madrid, E-28049 Madrid, Spain*

(Dated: May 20, 2025)

The relationship between antiferromagnetic (AFM) spin fluctuations (SF), nematic fluctuations, and superconductivity (SC) has been central to understanding the pairing mechanism in iron-based superconductors (IBSCs). Iron chalcogenides, which hold the simplest crystal structure in IBSCs, provide a good platform to investigate the relationship. Here, we report ^{77}Se and ^{125}Te nuclear magnetic resonance studies of $\text{FeSe}_{0.47}\text{Te}_{0.53}$, which is located close to a nematic quantum critical point (QCP), under pressures up to 1.35 GPa. Both the superconducting critical temperature and AFMSF were found to be enhanced under pressure, which suggests a correlation between SC and AFMSF in $\text{FeSe}_{0.47}\text{Te}_{0.53}$. However, the contribution of AFMSF to SC in $\text{FeSe}_{0.47}\text{Te}_{0.53}$ was found to be much less compared to that in $\text{FeSe}_{1-x}\text{S}_x$, suggesting that nematic fluctuations play a dominant role in the SC in $\text{FeSe}_{1-x}\text{Te}_x$ around the nematic QCP.

The interplay between magnetic fluctuations, electronic nematicity and the unconventional superconductivity (SC) has received wide interest after the discovery of SC in iron pnictides [1]. In many of the iron pnictide superconductors, by lowering temperature (T), the crystal structure changes from high- T tetragonal (C_4 symmetry) to low- T orthorhombic (C_2 symmetry) around a system-dependent Néel temperature T_N , below which long-range stripe-type antiferromagnetic (AFM) order emerges [2–4]. Nematicity is associated with this structural transition that breaks C_4 symmetry and is characterized by the development of in-plane anisotropy in the electronic properties. SC in these compounds emerges upon suppressing both the structural (or nematic) and magnetic transitions by carrier doping and/or applying pressure (p). Although this suggests a close relationship between AFM and nematic phases, it also makes a difficulty to separate the individual contribution to SC.

In this context, $\text{CaK}(\text{Fe}_{1-x}\text{M}_x)_4\text{As}_4$ ($M = \text{Co}, \text{Ni}, \text{Mn}, \text{Cr}$) is a rare and novel SC system which exhibits only AFM state called a hedgehog spin-vortex crystal (HSVC) without nematic phase transition [5–8]. From nuclear magnetic resonance (NMR) measurements, a possible HSVC AFM quantum critical point (QCP) has been reported around $x \sim 0$ where the AFM spin fluctuations (SF) play an important role in the appearance of SC [9].

The S or Te substituted FeSe system also provides a favorable platform for the study of the impact of nematicity or antiferromagnetism on SC independently [10–14]. In contrast to the $\text{CaK}(\text{Fe}_{1-x}\text{M}_x)_4\text{As}_4$ system, the superconductor FeSe ($x = 0$) with a critical temperature of $T_c = 8.5$ K exhibits only a nematic phase transition at $T_{\text{nem}} = 90$ K without AFM ordering at ambient p [10, 15, 16]. S or Te substitutions for Se in FeSe result in intriguing phase diagrams as shown in Fig. 1(a).

In the case of the S substitution, the nematic phase [the green region in Fig. 1(a)] is gradually suppressed

and disappears around a nematic QCP $x_{c,S} \sim 0.17$ [11]. In contrast, T_c first increases from $T_c = 8.5$ K up to 10 K around $x = 0.09$ [17–19], then drops to $T_c \sim 5$ K at $x_{c,S}$ without any enhancement of T_c around the nematic QCP [SC2 region in Fig. 1(a)]. Above $x_{c,S}$, T_c becomes nearly independent of x [SC1 region in Fig. 1(a)] and the fully replaced FeS is still a superconductor with $T_c = 5$ K [20]. As in the case of FeSe, no AFM state has been observed in $\text{FeSe}_{1-x}\text{S}_x$ at ambient p . Nevertheless, NMR measurements reveal clear correlations between T_c and nuclear spin-lattice relaxation rate $1/T_1$ [21–25], but in different ways in the C_2 and C_4 phases [26–32], showing the importance of spin fluctuations in $\text{FeSe}_{1-x}\text{S}_x$.

In the Te-substitution case, T_c initially decreases to a local minimum at $x \sim 0.3$ and then starts increasing towards the board maximum around $x = 0.6$, making two different SC regions (SC2 and SC3) as shown in Fig. 1(a) in $\text{FeSe}_{1-x}\text{Te}_x$ [14]. It is reported that, from the elastoresistivity and upper critical field measurements on $\text{FeSe}_{1-x}\text{Te}_x$, the enhancement of T_c is around the pure nematic critical point $x_{c,\text{Te}} \sim 0.5$ where the nematic phase disappears and a diverging nematic susceptibility was observed [14, 33, 34]. At very close to FeTe above $x \sim 0.9$, the AFM state with the bicollinear magnetic structure can be observed where T_N increases from 32 K at $x = 0.94$ to 76 K at $x = 1$ [35]. The two distinct SC regions were clearly demonstrated by applying magnetic field H [33]. At $\mu_0 H = 14$ T, T_c around $x = 0.3$ in $\text{FeSe}_{1-x}\text{Te}_x$ is strongly suppressed leading to two split SC regions originating from SC2 and SC3 (note SC1 is completely suppressed at this H) [33]. The SC2 regions shrunk leading to a SC dome in S-substituted region centered around $x = 0.1$ on $\text{FeSe}_{1-x}\text{S}_x$ with $T_c \sim 2$ K is observed, and it disappears completely at $\mu_0 H = 30$ T [33]. In contrast, the SC dome centered at $x = 0.6$ in $\text{FeSe}_{1-x}\text{Te}_x$ persists at 30 T and, survives even at $\mu_0 H = 46$ T at x close to the nematic QCP, suggesting that

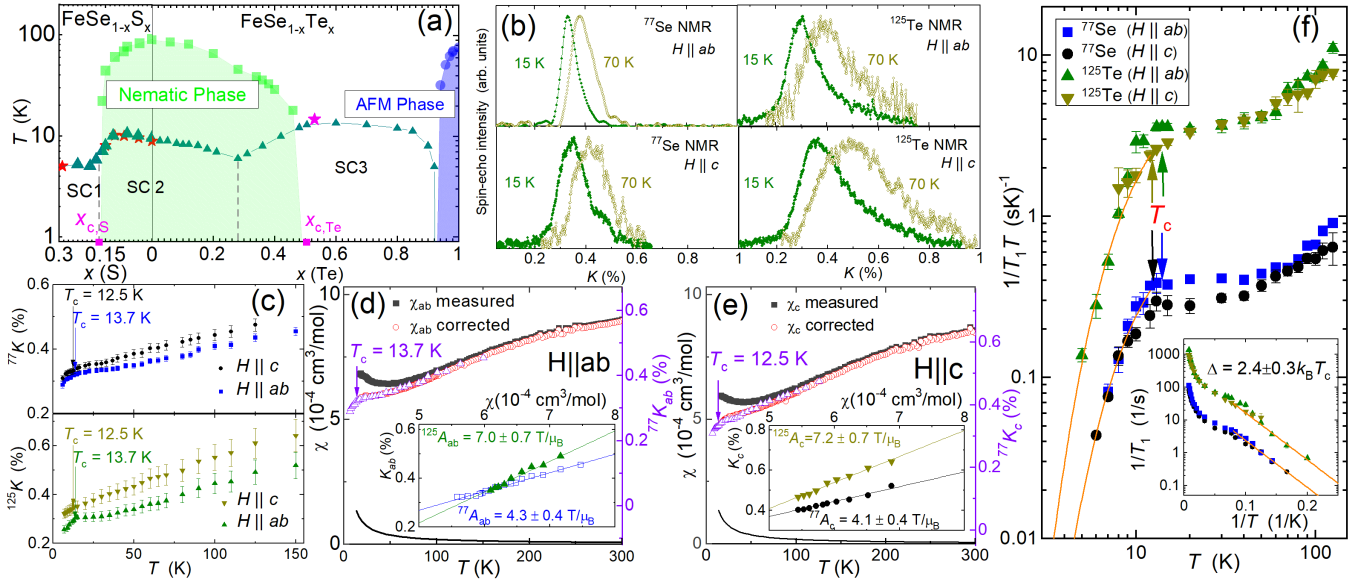


FIG. 1. (a) Phase diagrams in $\text{FeSe}_{1-x}\text{Te}_x$ and $\text{FeSe}_{1-x}\text{S}_x$ (note the vertical axis is in log-scale). x_c indicates the nematic QCP. SC1, SC2, and SC3 are three different SC regions [33]. The data in triangles (T_c) and squares (T_{nem}) are from Ref. [13], the data in circles (T_N) are from Ref. [35], and the data in stars (T_c) are from Ref. [25] and the present study. (b) ^{77}Se and ^{125}Te NMR spectra of $\text{FeSe}_{0.47}\text{Te}_{0.53}$ at $T = 15$ K and 70 K for $H \parallel ab$ and $H \parallel c$. (c) T dependencies of the ^{77}Se and ^{125}Te Knight shifts K . $\chi(T)$ and ^{77}K (right axes) for $H \parallel ab$ and $H \parallel c$ are shown in (d) and (e), respectively. The upturns in $\chi(T)$ below ~ 50 K are due to impurities that follow Curie behavior $\chi_{\text{imp}} = C/T$ with $C = 0.0018 \text{ cm}^3/\text{mol}$ for both directions, as shown in black lines. The open circles are corrected $\chi(T)$ by subtracting χ_{imp} (See text). Insets: $K(T)$ versus $\chi(T)$ for the corresponding ab and c components of K . The solid lines are linear fits. (f) T dependencies of ^{77}Se and ^{125}Te $1/T_1$. The inset shows the semi-log plot of $1/T_1$ vs. $1/T$. The orange solid curves below T_c are calculated results using a full-gap model.

nematic fluctuations play an important role in the appearance of SC in $\text{FeSe}_{1-x}\text{Te}_x$ near $x_{c,\text{Te}}$ [14, 33]. It is also interesting to point out that, although $\text{FeSe}_{1-x}\text{Te}_x$ has been studied less than $\text{FeSe}_{1-x}\text{S}_x$ due to its higher inhomogeneity originating from the difficulty in synthesizing $\text{FeSe}_{1-x}\text{Te}_x$ single crystals [36], $\text{FeSe}_{1-x}\text{Te}_x$ has been considered as one of the platforms for topological superconductivity, evidenced by scanning tunneling spectroscopy and angle-resolved photoemission spectroscopy measurements [37–41]. These characteristics also underline the importance of understanding the superconducting mechanism in $\text{FeSe}_{1-x}\text{Te}_x$.

It is therefore crucial to investigate in detail how the magnetic fluctuations correlate with T_c in $\text{FeSe}_{1-x}\text{Te}_x$. Usually, such studies can be performed by NMR measurements on different Te content samples with different T_c in $\text{FeSe}_{1-x}\text{Te}_x$. On the other hand, it has been shown that T_c largely depends on p in $\text{FeSe}_{1-x}\text{Te}_x$ [13], which provides a good opportunity to study it without changing samples. In this Letter, we report the results of ^{77}Se and ^{125}Te NMR measurements on $\text{FeSe}_{0.47}\text{Te}_{0.53}$, which is close to the nematic QCP [Fig. 1(a)], to investigate the relationship between SC, nematic fluctuations, and AFMSF. Owing to the sensitivity of T_c on p , by carrying out NMR measurements up to 1.35 GPa, we found that the contribution of AFMSF to SC in $\text{FeSe}_{0.47}\text{Te}_{0.53}$ is much less compared to that in $\text{FeSe}_{1-x}\text{S}_x$, and nematic fluctuations can be the source of SC in $\text{FeSe}_{0.47}\text{Te}_{0.53}$.

Single crystals of $\text{FeSe}_{0.47}\text{Te}_{0.53}$ ($T_c = 14.7$ K at ambient p under $H = 0$) were prepared using the chemical vapor transport technique following Ref. [14], and details are given in the Supplemental Materials (SM) [42]. ^{125}Te ($I = 1/2$, $\gamma_N/2\pi = 13.454 \text{ MHz/T}$) NMR was measured at ambient p , while ^{77}Se ($I = 1/2$, $\gamma_N/2\pi = 8.118 \text{ MHz/T}$) NMR was measured up to 1.35 GPa [43]. NMR spectra were obtained by sweeping frequency at $\mu_0 H = 7.4089$ T or sweeping H at constant frequencies. $1/T_1$ was measured with a saturation recovery method [46]. T_c was determined by ac susceptibility measurements [42]. Magnetic susceptibility was measured at $\mu_0 H = 7$ T using a SQUID magnetometer (Quantum Design, MPMS).

Figure 1(b) shows the typical ^{77}Se and ^{125}Te NMR spectra of $\text{FeSe}_{0.47}\text{Te}_{0.53}$ in the normal state at $T = 15$ K and 70 K for H parallel to the ab plane ($H \parallel ab$) and H parallel to the c axis ($H \parallel c$) ($T_c = 13.7$ K (12.5 K) under $H \parallel ab$ ($H \parallel c$) of 7.4089 T [42]). All spectra observed are a little asymmetric, which could be due to a slight distribution of the hyperfine coupling constants A of the Se and Te sites. The full width at half maximum (FWHM) of the ^{77}Se NMR spectra decrease almost linearly from 85 and 120 Oe at 100 K to 53 and 94 Oe at 15 K for $H \parallel ab$ and $H \parallel c$, respectively. A similar T dependence of the FWHM is observed in the ^{125}Te NMR spectra where the FWHM decreases from 183 and 242 Oe at 100 K to 100 and 137 Oe at 15 K for $H \parallel ab$ and $H \parallel c$, respectively. The FWHM of ^{125}Te NMR spectra

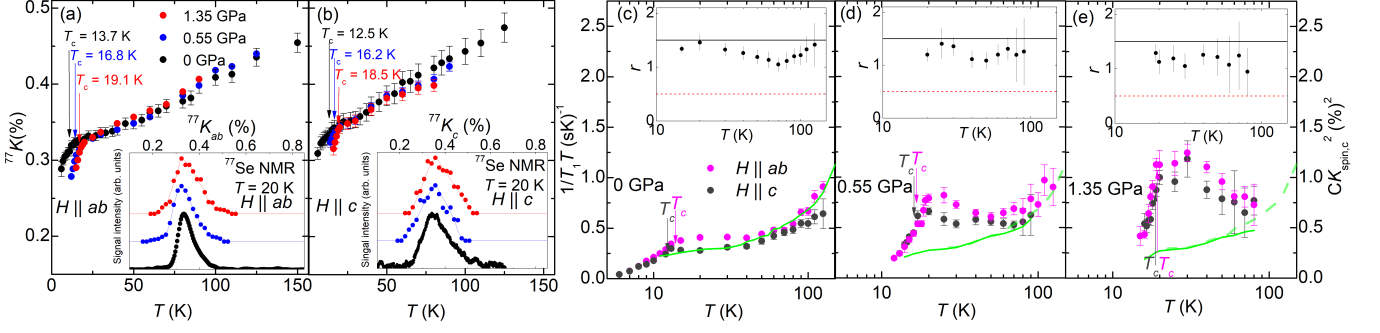


FIG. 2. T dependencies of the ^{77}Se K_{ab} (a) and K_c (b) under various p . Downward arrows indicate T_c under $\mu_0 H = 7.4089$ T for each H direction. Insets show the ^{77}Se NMR spectra at $T = 20$ K under various p for $H \parallel ab$ (a) and $H \parallel c$ (b). (c)-(e) T dependencies of ^{77}Se NMR $1/T_1 T$ (left axes) at various p with $H \parallel ab$ (magenta circles) and $H \parallel c$ (gray circles). The arrows indicate T_c under 7.4089 T [42]. The green curve for each panel (right axes) shows the T dependence of $CK_{\text{spin},c}^2$, where $K_{\text{spin},c}$ is the spin part of K_c estimated by subtracting the T -independent K_0 and C is a scaling factor. For all p , 0.175% and 9.5 are used for K_0 and C , respectively. The insets in (c)-(e) show the T dependence of the ratio $r \equiv (1/T_1 T)_{ab}/(1/T_1 T)_c$. The two horizontal lines represent the expected values for stripe-type ($r = 1.5$) and Néel-type ($r = 0.5$) AFMSFs, respectively.

is 1.5-2.1 as large as that of ^{77}Se NMR spectra, which is mainly due to the different A , as shown below. It is also noted that the FWHM of the ^{77}Se NMR spectra in $\text{FeSe}_{0.47}\text{Te}_{0.53}$ are 3~5 times that in $\text{FeSe}_{0.0.71}\text{Te}_{0.29}$, due to the higher inhomogeneity in $\text{FeSe}_{1-x}\text{Te}_x$ as mentioned above (See the comparison in SM).

The T dependencies of ^{77}Se and ^{125}Te Knight shifts (^{77}K and ^{125}K) under $H \parallel ab$ (K_{ab}) and $H \parallel c$ (K_c) are shown in Fig. 1(c). Both K_{ab} and K_c for ^{77}Se and ^{125}Te nuclei decrease with decreasing T and exhibit further reduction below T_c , suggesting a spin-singlet SC state. This T dependence is qualitatively consistent with previous studies on similar compounds of $x = 0.58$ [47], 0.5 [48], 0.67 [49], and 0.6 [50] in $\text{FeSe}_{1-x}\text{Te}_x$. The T dependencies of K_{ab} and K_c of ^{77}Se and ^{125}Te are also consistent with those of the magnetic susceptibilities $\chi(T)$ shown in Figs. 1(d) and 1(e), except for the low T where the upturns were observed. The upturns in $\chi(T)$ at low T , therefore, can be not intrinsic and arise from a small amount of paramagnetic impurities. The impurity contributions were assumed to be of Curie form and were subtracted from the observed $\chi(T)$ so as to match the T dependencies of ^{77}K with the corrected $\chi(T)$ shown by open circles [see Figs. 1(d) and 1(e)]. In fact, the linear relation between the Knight shifts K and the corrected χ can be seen in the insets of Figs. 1(d) and 1(e) where K_{ab} and K_c for ^{77}Se and ^{125}Te are plotted against the corresponding corrected χ_{ab} and χ_c , respectively.

As K is the sum of the T -dependent spin part K_{spin} and a T -independent orbital part K_0 (that is, $K(T) = K_0 + K_{\text{spin}}$) and K_{spin} is proportional to the spin susceptibility χ_{spin} through the hyperfine coupling constants A , the slope provides an estimate of A . From those slopes, the values of A for ^{125}Te (^{77}Se) are estimated to be $^{125}A_{ab} = 7.0(7)$ T/ μ_B ($^{77}A_{ab} = 4.3(4)$ T/ μ_B) and $^{125}A_c = 7.2(7)$ T/ μ_B ($^{77}A_c = 4.1(4)$ T/ μ_B) for $H \parallel ab$ and $H \parallel c$, respectively. These A values are greater than the $^{125}A_{ab} = 3.63$ T/ μ_B and $^{125}A_c = 4.88$ T/ μ_B ($^{77}A_c = 2.85$ T/ μ_B)

in $\text{Fe}_{1.04}\text{Se}_{0.33}\text{Te}_{0.67}$ [49] but are comparable to $^{77}A_{ab} = 3.585$ T/ μ_B and $^{77}A_c = 4.37$ T/ μ_B in FeSe [25].

To investigate the dynamical properties of the compound, we measured $1/T_1 T$ for both nuclei under the two H directions whose results are shown in Fig. 1(f). Although the $1/T_1 T$ values of ^{77}Se and ^{125}Te are different due to the difference in the A values and the nuclear gyromagnetic ratio, $1/T_1 T$ for both nuclei shows a similar T dependence where $1/T_1 T$ decreases as T decreases and becomes nearly constant below ~ 50 K within our experimental uncertainty. Below T_c (shown by arrows in Fig. 1(f)), $1/T_1 T$'s for both nuclei decrease exponentially due to the opening of SC gap, which may suggest a fully gapped SC state. In fact, as shown in the inset of Fig. 1(f), an exponential decrease of $1/T_1$ can be seen in the semi-log plot of $1/T_1$ vs. $1/T$ from which the gap magnitude is estimated to be $\Delta/k_B T_c = 2.4(3)$ within our experimental T range measured. A similar exponential behavior of $1/T_1$ in the SC state has been reported in $\text{FeSe}_{0.42}\text{Te}_{0.58}$ with a slightly larger gap magnitude of $\Delta/k_B T_c = 3.0$ [47]. The STM measurements also show a full-gap SC in optimally Te substituted FeSe [51]. However, the SC-gap structure is still controversial. A nodal gap structure has been suggested from ^{125}Te NMR measurements in $\text{Fe}_{1.04}\text{Se}_{0.33}\text{Te}_{0.67}$ where $1/T_1 \propto T^5$ just below T_c has been reported [49]. In addition, a SC state with multiple full gaps has been observed in $\text{FeSe}_{0.45}\text{Te}_{0.55}$ by the later STM study [52]. Further studies are required to clarify the SC gap structure of $\text{FeSe}_{1-x}\text{Te}_x$ around $x = 0.5$ -0.6.

Now we discuss the magnetic fluctuations in the normal state, focusing on how it changes with p because T_c largely depends on p [13, 42]. For this purpose, we carried out ^{77}Se NMR measurements under p of 0.55 and 1.35 GPa which leads to an increase in T_c from 14.7 K at ambient p to 17.6 K at 0.55 GPa, and to 19.8 K at 1.35 GPa at $H = 0$ (see details in the SM [42]). Since ^{125}Te - $1/T_1 T$ and ^{77}Se - $1/T_1 T$ show a similar T depen-

dence as described above, here we discuss the SFs using only ^{77}Se - $1/T_1T$ data. Generally, $1/T_1T$ is related to the \mathbf{q} -sum dynamical magnetic susceptibility, while the NMR shift K measures the uniform magnetic susceptibility $\chi'(\mathbf{q} = 0, \omega_N = 0)$. Therefore, by comparing the T dependence of $1/T_1T$ and K , one can obtain insight into the T evolution of $\sum_{\mathbf{q}} \chi''(\mathbf{q}, \omega_N)$ with respect to that of $\chi'(0, 0)$. To obtain the T dependence of NMR shift at different pressures, we measured ^{77}Se NMR spectra of $\text{FeSe}_{0.47}\text{Te}_{0.53}$ (see typical observed spectra shown in the insets in Fig. 2) under p . The obtained T and p dependencies of the $^{77}K_{ab}$ and $^{77}K_c$ are shown in Figs. 2(a) and 2(b), respectively, showing that $^{77}K_{ab}$ and $^{77}K_c$ are nearly p independent. Given the nearly p -independent values of $1/T_1T$ at high-temperature region as described below, together with the nearly p -independent behavior of Knight shift, the hyperfine coupling constants are considered to be nearly p -independent up to at least 1.35 GPa, as in the case of the isostructural $\text{FeSe}_{1-x}\text{S}_x$ [26–31]. It is interesting to point out that, since K is proportional to the density of states at the Fermi energy $N(E_F)$, the results indicate that $N(E_F)$ is nearly independent of p , although T_c changes significantly. This is in contrast to conventional BCS superconductors, in which $N(E_F)$ generally correlates with T_c . These results suggest that the SC in $\text{FeSe}_{1-x}\text{Te}_x$ is unconventional rather than conventional which is consistent with the results of the Raman spectroscopy measurements that reveal the strength of electron-phonon coupling is insufficient to produce $T_c \sim 14$ K in $\text{FeSe}_{0.4}\text{Te}_{0.6}$ [53].

Here we compare the T dependencies of $1/T_1T$ with those of K . Figures 2(c)–2(e) display the T dependencies of $1/T_1T$ for both $H \parallel ab$ and $H \parallel c$ at ambient pressure, 0.55 GPa, and 1.35 GPa, respectively. At ambient p as described above, there is a qualitative similarity in the T dependencies of $1/T_1T$ and K above ~ 40 K. However, below this T , one can see the different T dependence between $1/T_1T$ and K where $1/T_1T$ for both field directions becomes nearly constant, while K_{ab} and K_c keep decreasing as shown in Fig. 2(a) and 2(b). The deviation at low T can be attributed to the development of AFMSF with $\mathbf{q} \neq 0$. Interestingly, at $p = 0.55$ GPa, the large enhancements in $1/T_1T$ are observed at low T below ~ 60 K although less p effects were detected at high T . A further enhancement in $1/T_1T$ at low T can be seen at $p = 1.35$ GPa, indicating a strong enhancement of the AFMSF under pressure [54]. According to previous NMR studies performed on IBSCs and their related materials [55–60], one can obtain the information on the nature of SFs from the ratio $r \equiv T_{1,c}/T_{1,ab}$. In most IBSCs, r has been found to be ~ 1.5 , corresponding to the stripe-type AFMSF with $\mathbf{q} = (\pi, 0)$ or $(0, \pi)$. On the other hand, $r = 0.5$ is expected for $\mathbf{q} = (\pi, \pi)$ spin correlations. Note the wave vectors are given in the single-iron Brillouin zone notation. As shown in the insets in Figs. 2(c)–(e), r is in the range of $1 \sim 1.5$ for all the pressures, but never decreases to 0.5. This suggests that the AFMSFs are characterized with $\mathbf{q} = (\pi, 0)$ or $(0, \pi)$. This is con-

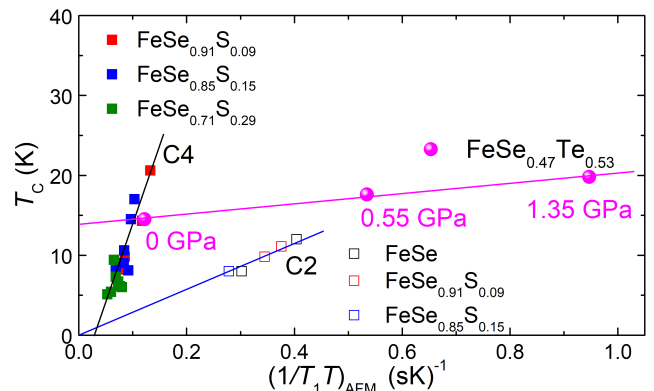


FIG. 3. Plot of T_c at zero field vs $(1/T_1T)_{\text{AFM}}$. $(1/T_1T)_{\text{AFM}}$ value is taken at T around 20 \sim 30 K in $\text{FeSe}_{0.47}\text{Te}_{0.53}$ and $T = 15$ K in $\text{FeSe}_{1-x}\text{S}_x$ from Refs. [26, 28]. Black and blue lines show linear fits for the C_4 (closed symbols) and C_2 (open symbols) phases of $\text{FeSe}_{1-x}\text{S}_x$, respectively.

sistent with the inelastic neutron scattering study which revealed dominant stripe-type AFMSF below ~ 100 K in $\text{FeSe}_{1-x}\text{Te}_x$ although bicollinear stripe-type AFMSF also contribute at higher T above 100 K [61].

To explore the relationship between the magnitude of AFMSF and T_c , we follow our previous papers for $\text{FeSe}_{1-x}\text{S}_x$ [26–28] where the observed $1/T_1T$ was decomposed into the two contributions: \mathbf{q} -independent component $(1/T_1T)_0$ and AFM component $(1/T_1T)_{\text{AFM}}$. $(1/T_1T)_0$ is expected to be proportional to K_{spin}^2 . Therefore, by comparing the observed $1/T_1T$ with K_{spin}^2 , $(1/T_1T)_{\text{AFM}}$ can be estimated. Since $(1/T_1T)_{ab}$ is enhanced more than $(1/T_1T)_c$, which is expected for the case of stripe-type AFM spin correlations, we compare the $(1/T_1T)_{ab}$ with K_c . The green curve for each panel (right axes) in Figs. 2(c)–(e) shows the T dependence of $CK_{\text{spin},c}^2$, where C is a scaling factor. At ambient p , a good scaling between $1/T_1T$ and $CK_{\text{spin},c}^2$ at high T can be seen in Fig. 2(c), using $K_0 = 0.175\%$ and $C = 9.5$. Those values seem to be reasonable as similar C values (7.75–8.5) and the same K_0 have been reported in $\text{FeSe}_{1-x}\text{S}_x$ [26, 28]. Since there is no clear change in K_c with pressure, we used the same values of K_0 and C for $p = 0.55$ and 1.35 GPa. Thus, the differences between $(1/T_1T)_{ab}$ (magenta circles) and the green curves are attributed to the contributions of AFM spin fluctuations, $(1/T_1T)_{\text{AFM}}$.

Figure 3 presents the relationship between T_c under zero H and the magnitude of AFMSF under different p . Here the magnitudes of AFMSF are represented by the values of $(1/T_1T)_{\text{AFM}}$ just above T_c . For comparison, data from previous studies for $\text{FeSe}_{1-x}\text{S}_x$ were also plotted in Fig. 3 [26–28]. In $\text{FeSe}_{1-x}\text{S}_x$, it was revealed that T_c is proportional to AFMSFs in the C_4 (closed symbols) and C_2 (open symbols) phases as shown by black and blue lines, respectively [26, 28]. It was also pointed out that the slope for the C_4 phase is steeper than that for the

C_2 state, indicating that the AFMSFs without nematicity enhance T_c more than those with nematicity [26, 28]. The origin of different slopes has been discussed in terms of the different numbers of hotspots on Fermi surfaces with and without nematicity [28, 62]. Interestingly, both the C_2 and C_4 lines for $\text{FeSe}_{1-x}\text{S}_x$ start from around the origin in the plot, suggesting the SC in $\text{FeSe}_{1-x}\text{S}_x$ is mainly induced by AFMSFs.

In the case of $\text{FeSe}_{0.47}\text{Te}_{0.53}$, both the AFMSFs and T_c enhance with p and a linear relationship between them is found as shown by the magenta line in Fig. 3. However, the slope of this relationship is quite different from those observed in $\text{FeSe}_{1-x}\text{S}_x$. The small slope cannot be simply explained by the number of hotspots as the Fermi surface topology of the very close compound $\text{FeSe}_{0.45}\text{Te}_{0.55}$ [41] has been reported to be very similar to the case of the C_4 phase in $\text{FeSe}_{1-x}\text{S}_x$ [28]. Thus the smaller slope indicates that AFMSFs do not contribute significantly to the SC in $\text{FeSe}_{0.47}\text{Te}_{0.53}$, which is quite different from the case of $\text{FeSe}_{1-x}\text{S}_x$. Furthermore, the intercept of the magenta line in the plot is significantly away from the origin, indicating a high residual T_c value even as AFMSFs approach zero. This behavior implies that the mechanism of SC in $\text{FeSe}_{0.47}\text{Te}_{0.53}$ is not primarily driven by AFMSFs but likely has another origin which would be naturally attributed to nematic fluctuations. This interpretation aligns with the observation of a pure nematic QCP and the enhancement of the SC pairing strength near this nematic QCP [14, 33].

Recently the importance of nematicity or nematic fluctuations has been actually pointed out in many IBSCs [10, 11, 13, 24, 63–72]. For example, in $\text{LiFe}_{1-x}\text{Co}_x\text{As}$, the strongest spin fluctuations were observed in the sample around $x \sim 0.12$, far from the maximum T_c position [64]. In addition, in the highly-doped $\text{LaFeAsO}_{1-x}\text{F}_x$, AFMSFs are found to be weak but T_c is high [65]. These results imply a different SC mechanism other than AFMSF. The close relation between

enhanced pairing and nematic fluctuations was observed in $\text{Ba}_{1-x}\text{Sr}_x\text{Ni}_2\text{As}_2$ [71]. Furthermore, the suppression of T_c by anisotropic strain near a nematic QCP in $\text{Ba}(\text{Fe}_{1-x}\text{Co}_x)_2\text{As}_2$ [69] also provides strong evidence of the SC driven by nematic fluctuations. Nevertheless, the relationship between the magnitude of nematic fluctuations and T_c seems not yet well established. Therefore, our findings strongly call for further detailed investigation of the relationship in not only $\text{FeSe}_{0.47}\text{Te}_{0.53}$ under pressure but also other systems. Such studies utilizing nematicity sensitive measurements including elastoresistivity and Nernst measurements [73] will be essential to elucidate the contributions of nematic fluctuations to SC in unconventional SCs.

In summary, high pressure NMR measurements of ^{77}Se and ^{125}Te have been performed on $\text{FeSe}_{0.47}\text{Te}_{0.53}$, which is close to a nematic QCP. By comparing the correlations between the magnitude of AFM spin fluctuations and T_c in $\text{FeSe}_{0.47}\text{Te}_{0.53}$ and $\text{FeSe}_{1-x}\text{S}_x$, nematic fluctuations were suggested to play an important role for the SC in $\text{FeSe}_{0.47}\text{Te}_{0.53}$. The different contributions of AFMSF to SC in S and Te substituted FeSe were pointed out to be the origin of the different behavior of T_c around nematic QCP for each system [33]. Our results under pressure highlight the $\text{FeSe}_{1-x}\text{Te}_x$ system as a very suitable platform to study the role of nematic fluctuations on SC, stimulating further investigations of the system under pressure, and also provide insights into the mechanism of unconventional superconductivity. Systematic NMR measurements at ambient and under pressure on $\text{FeSe}_{1-x}\text{Te}_x$ with different Te contents below and above the nematic QCP are in progress.

We would like to acknowledge C. L. Mueller for assistance in the preparation of the crystals. The research was supported by the U.S. Department of Energy (DOE), Office of Basic Energy Sciences, Division of Materials Sciences and Engineering. Ames National Laboratory is operated for the U.S. DOE by Iowa State University under Contract No. DE-AC02-07CH11358.

-
- [1] Y. Kamihara, T. Watanabe, M. Hirano, and H. Hosono, Iron-Based Layered Superconductor $\text{La}[\text{O}_{1-x}\text{F}_x]\text{FeAs}$ ($x = 0.05\text{--}0.12$) with $T_c = 26$ K, *J. Am. Chem. Soc.* **130**, 3296 (2008).
 - [2] D. C. Johnston, The puzzle of high temperature superconductivity in layered iron pnictides and chalcogenides, *Adv. Phys.* **59**, 803 (2010).
 - [3] P. C. Canfield and S. L. Bud'ko, FeAs-Based Superconductivity: A Case Study of the Effects of Transition Metal Doping on BaFe_2As_2 , *Annu. Rev. Condens. Matter Phys.* **1**, 27 (2010).
 - [4] G. R. Stewart, Superconductivity in iron compounds, *Rev. Mod. Phys.* **83**, 1589 (2011).
 - [5] J. Cui, Q.-P. Ding, W. R. Meier, A. E. Böhmer, T. Kong, V. Borisov, Y. Lee, S. L. Bud'ko, R. Valentí, P. C. Canfield, and Y. Furukawa, Magnetic fluctuations and superconducting properties of $\text{CaKFe}_4\text{As}_4$ studied by ^{75}As NMR, *Phys. Rev. B* **96**, 104512 (2017).
 - [6] W. R. Meier, Q.-P. Ding, A. Kreyssig, S. L. Bud'ko, A. Sapkota, K. Kothapalli, V. Borisov, R. Valentí, C. D. Batista, P. P. Orth, R. M. Fernandes, A. I. Goldman, Y. Furukawa, A. E. Böhmer, and P. C. Canfield, Hedgehog spin-vortex crystal stabilized in a hole-doped iron-based superconductor, *npj Quantum Mater.* **3**, 5 (2018).
 - [7] J.M. Wilde, A. Sapkota, Q.P. Ding, M. Xu, W. Tian, S.L. Bud'ko, Y. Furukawa, A. Kreyssig, P.C. Canfield, Antiferromagnetic order and its interplay with superconductivity in $\text{CaK}(\text{Fe}_{1-x}\text{Mn}_x)_4\text{As}_4$, *J. Phys.: Condens. Matter* **35**, 395801 (2023).
 - [8] M. Xu, J. Schmidt, M. A. Tanatar, R. Prozorov, S. L. Bud'ko, and P. C. Canfield, Superconductivity and magnetic and transport properties of single-crystalline $\text{CaK}(\text{Fe}_{1-x}\text{Cr}_x)_4\text{As}_4$, *Phys. Rev. B* **107**, 134511 (2023).
 - [9] Q.-P. Ding, W. R. Meier, J. Cui, M. Xu, A. E. Böhmer, S.

- L. Bud'ko, P. C. Canfield, and Y. Furukawa, Hedgehog Spin-Vortex Crystal Antiferromagnetic Quantum Criticality in $\text{CaK}(\text{Fe}_{1-x}\text{Ni}_x)_4\text{As}_4$ Revealed by NMR, *Phys. Rev. Lett.* **121**, 137204 (2018).
- [10] A. E. Böhmer and A. Kreisel, Nematicity, magnetism and superconductivity in FeSe, *J. Phys. Condens. Matter* **30**, 023001 (2018).
- [11] S. Hosoi, K. Matsuura, K. Ishida, H. Wang, Y. Mizukami, T. Watashige, S. Kasahara, Y. Matsuda, and T. Shibauchi, Nematic quantum critical point without magnetism in $\text{FeSe}_{1-x}\text{S}_x$ superconductors, *Proc. Natl. Acad. Sci. USA* **113**, 8139 (2016).
- [12] A. I. Coldea, S. F. Blake, S. Kasahara, A. A. Haghighirad, M. D. Watson, W. Knafo, E. S. Choi, A. McCollam, P. Reiss, T. Yamashita, M. Bruma, S. Speller, Y. Matsuda, T. Wolf, T. Shibauchi, and A. J. Schofield, Evolution of the Fermi surface of the nematic superconductors $\text{FeSe}_{1-x}\text{S}_x$, *Npj Quant. Mater.* **4**, 2 (2019).
- [13] K. Mukasa, K. Matsuura, M. Qiu, M. Saito, Y. Sugimura, K. Ishida, M. Otani, Y. Onishi, Y. Mizukami, K. Hashimoto, J. Gouchi, R. Kumai, Y. Uwatoko, and T. Shibauchi, High-pressure phase diagrams of $\text{FeS}_{1-x}\text{Te}_x$: Correlation between suppressed nematicity and enhanced superconductivity, *Nat. Commun.* **12**, 381 (2021).
- [14] K. Ishida, Y. Onishi, M. Tsujii, K. Mukasa, M. Qiu, M. Saito, Y. Sugimura, K. Matsuura, Y. Mizukami, K. Hashimoto, and T. Shibauchi, Pure Nematic Quantum Critical Point Accompanied by a Superconducting Dome, *Proc. Natl. Acad. Sci. U.S.A.* **119**, e2110501119 (2022).
- [15] F.-C. Hsu, J.-Y. Luo, K.-W. Yeh, T.-K. Chen, T.-W. Huang, P. M. Wu, Y.-C. Lee, Y.-L. Huang, Y.-Y. Chu, D.-C. Yan, and M.-K. Wu, Superconductivity in the PbO-type structure α -FeSe, *Proc. Natl. Acad. Sci. U.S.A.* **105**, 14262 (2008).
- [16] T. M. McQueen, A. J. Williams, P. W. Stephens, J. Tao, Y. Zhu, V. Ksenofontov, F. Casper, C. Felser, and R. J. Cava, Tetragonal-to-Orthorhombic Structural Phase Transition at 90 K in the Superconductor $\text{Fe}_{1.01}\text{Se}$, *Phys. Rev. Lett.* **103**, 057002 (2009).
- [17] M. Abdel-Hafez, Y.-Y. Zhang, Z.-Y. Cao, C.-G. Duan, G. Karapetrov, V. M. Pudalov, V. A. Vlasenko, A. V. Sadakov, D. A. Knyazev, T. A. Romanova, D. A. Chareev, O. S. Volkova, A. N. Vasiliev, and X.-J. Chen, Superconducting properties of sulfur-doped iron selenide, *Phys. Rev. B* **91**, 165109 (2015).
- [18] M. D. Watson, T. K. Kim, A. A. Haghighirad, S. F. Blake, N. R. Davies, M. Hoesch, T. Wolf, and A. I. Coldea, Suppression of orbital ordering by chemical pressure in $\text{FeSe}_{1-x}\text{S}_x$, *Phys. Rev. B* **92**, 121108(R) (2015).
- [19] P. Reiss, M. D. Watson, T. K. Kim, A. A. Haghighirad, D. N. Woodruff, M. Bruma, S. J. Clarke, and A. I. Coldea, Suppression of electronic correlations by chemical pressure from FeSe to FeS, *Phys. Rev. B* **96**, 121103(R) (2017).
- [20] X. Lai, H. Zhang, Y. Wang, X. Wang, X. Zhang, J. Lin, and F. Huang, Observation of Superconductivity in Tetragonal FeS, *J. Am. Chem. Soc.*, **137** 10148 (2015).
- [21] A. E. Böhmer, T. Arai, F. Hardy, T. Hattori, T. Iye, T. Wolf, H. v. Löhneysen, K. Ishida, and C. Meingast, Origin of the Tetragonal-to-Orthorhombic Phase Transition in FeSe: A Combined Thermodynamic and NMR Study of Nematicity, *Phys. Rev. Lett.* **114**, 027001 (2015).
- [22] S.-H. Baek, D.V. Efremov, J.M. Ok, J.S. Kim, J. van den Brink, and B. Büchner, Orbital-driven nematicity in FeSe, *Nat. Mater.* **14**, 210 (2015).
- [23] T. Imai, K. Ahilan, F. L. Ning, T. M. McQueen, and R. J. Cava, Why Does Undoped FeSe Become a High- T_c Superconductor under Pressure? *Phys. Rev. Lett.* **102**, 177005 (2009).
- [24] P. Wiecki, M. Nandi, A. E. Böhmer, S. L. Bud'ko, P. C. Canfield, and Y. Furukawa, NMR evidence for static local nematicity and its cooperative interplay with low-energy magnetic fluctuations in FeSe under pressure, *Phys. Rev. B* **96**, 180502(R) (2017).
- [25] P. Wiecki, K. Rana, A. E. Böhmer, Y. Lee, S. L. Bud'ko, P. C. Canfield, and Y. Furukawa, Persistent correlation between superconductivity and antiferromagnetic fluctuations near a nematic quantum critical point in $\text{FeSe}_{1-x}\text{S}_x$, *Phys. Rev. B* **98**, 020507(R) (2018).
- [26] K. Rana, L. Xiang, P. Wiecki, R. A. Ribeiro, G. G. Lesseux, A. E. Böhmer, S. L. Bud'ko, P. C. Canfield, and Y. Furukawa, impact of nematicity on the relationship between antiferromagnetic fluctuations and superconductivity in $\text{FeSe}_{0.91}\text{S}_{0.09}$ under pressure, *Phys. Rev. B* **101**, 180503(R) (2020).
- [27] K. Rana, and Y. Furukawa, Relationship between Nematicity, Antiferromagnetic Fluctuations, and Superconductivity in $\text{FeSe}_{1-x}\text{S}_x$ revealed by NMR, *Front. Phys.* **10**, 849284 (2022).
- [28] K. Rana, D. V. Ambika, S. L. Bud'ko, A. E. Böhmer, P. C. Canfield, and Y. Furukawa, Interrelationships between nematicity, antiferromagnetic spin fluctuations, and superconductivity: Role of hotspots in $\text{FeSe}_{1-x}\text{S}_x$ revealed by high pressure ^{77}Se NMR study, *Phys. Rev. B* **107**, 134507 (2023).
- [29] T. Kuwayama, K. Matsuura, Y. Mizukami, S. Kasahara, Y. Matsuda, T. Shibauchi, Y. Uwatoko, and N. Fujiwara, NMR study under pressure on the iron-based superconductor $\text{FeSe}_{1-x}\text{S}_x$ ($x = 0.12$ and 0.23): Relationship between nematicity and AF fluctuations, *Mod. Phys. Lett. B* **34**, 2040048 (2020).
- [30] T. Kuwayama, K. Matsuura, J. Gouchi, Y. Yamakawa, Y. Mizukami, S. Kasahara, Y. Matsuda, T. Shibauchi, H. Kontani, Y. Uwatoko and N. Fujiwara, Pressure-induced reconstitution of Fermi surfaces and spin fluctuations in S-substituted FeSe, *Sci. Rep.* **11**, 17265 (2021).
- [31] T. Kuwayama, K. Matsuura, Y. Mizukami, S. Kasahara, Y. Matsuda, T. Shibauchi, Y. Uwatoko and N. Fujiwara, ^{77}Se -NMR Study under Pressure on 12%-S Doped FeSe, *J. Phys. Soc. Jpn.* **88**, 033703 (2019).
- [32] Z. Yu, K. Nakamura, K. Inomata, X. Shen, T. Mikuri, K. Matsuura, Y. Mizukami, S. Kasahara, Y. Matsuda, T. Shibauchi *etal.*, Spin fluctuations from Bogoliubov Fermi surfaces in the superconducting state of S-substituted FeSe, *Commun. Phys.* **6**, 175 (2023).
- [33] K. Mukasa, K. Ishida, S. Imajo, M. Qiu, M. Saito, K. Matsuura, Y. Sugimura, S. Liu, Y. Uezono, T. Otsuka, M. Čulo, S. Kasahara, Y. Matsuda, N. E. Hussey, T. Watanabe, K. Kindo, and T. Shibauchi, Enhanced Superconducting Pairing Strength near a Pure Nematic Quantum Critical Point, *Phys. Rev. X* **13**, 011032 (2023).
- [34] Q. Jiang, Y. Shi, M. H. Christensen, J. Sanchez, B. Huang, Z. Lin, Z. Liu, P. Malinowski, X. Xu, R. M. Fernandes, and J.-H. Chu, Nematic fluctuations in an orbital selective superconductor $\text{Fe}_{1+y}\text{Te}_{1-x}\text{Se}_x$. *Commun. Phys.* **6**, 39 (2023).
- [35] T. Otsuka, S. Hagiwara, Y. Koshika, S. Adachi, T. Usui, N. Sasaki, S. Sasaki, S. Yamaguchi, Y. Nakanishi, M.

- Yoshizawa, S. Kimura, and T. Watanabe, Incoherent-coherent crossover and the pseudogap in Te-annealed superconducting $\text{Fe}_{1+y}\text{Te}_{1-x}\text{Se}_x$ revealed by magnetotransport measurements, *Phys. Rev. B* **99**, 184505 (2019).
- [36] Q. Hou, L. Sun, Y. Sun, and Z. Shi, Review of Single Crystal Synthesis of 11 Iron-Based Superconductors, *Materials* **16**, 4895 (2023).
- [37] J. X. Yin, Z. Wu, and J. H. Wang *et al.*, Observation of a robust zero-energy bound state in iron-based superconductor $\text{Fe}(\text{Te},\text{Se})$, *Nat. Phys.* **11**, 543 (2015).
- [38] D. Wang, L. Kong, and P. Fan *et al.*, Evidence for Majorana bound states in an iron-based superconductor, *Science* **362**, 333 (2018).
- [39] T. Machida, Y. Sun, S. Pyon, S. Takeda, Y. Kohsaka, T. Hanaguri, T. Sasagawa, and T. Tamegai, Zero-energy vortex bound state in the superconducting topological surface state of $\text{Fe}(\text{Se},\text{Te})$, *Nat. Mater.* **18**, 811 (2019).
- [40] P. Zhang, K. Yaji, and T. Hashimoto *et al.*, Observation of topological superconductivity on the surface of an iron-based superconductor, *Science* **360**, 182 (2018).
- [41] Y.-F. Li, S.-D. Chen, M. García-Díez, M. I. Iraola, H. Pfau, Y.-L. Zhu, Z.-Q. Mao, T. Chen, M. Yi, P.-C. Dai, J. A. Sobota, M. Hashimoto, M. G. Vergniory, D.-H. Lu, and Z.-X. Shen, Orbital Ingredients and Persistent Dirac Surface State for the Topological Band Structure in $\text{FeTe}_{0.55}\text{Se}_{0.45}$, *Phys. Rev. X* **14**, 021043 (2024).
- [42] See Supplemental material for the details of sample preparation, EDS measurements, the results of the ac susceptibility measurements, the comparison of the ^{77}Se NMR spectra to those of $\text{FeSe}_{0.71}\text{S}_{0.29}$, NMR pulse conditions in the SC state, and the typical relaxation curves for ^{77}Se T_1 measurements.
- [43] The pressure was applied with a NiCrAl/CuBe piston-cylinder cell using Daphne 7373 as the pressure transmitting medium. Pressure calibration was accomplished by ^{63}Cu nuclear quadrupole resonance in Cu_2O [44, 45] at 77 K.
- [44] A. P. Reyes, E. T. Ahrens, R. H. Heffner, P. C. Hammel, and J. D. Thompson, Cuprous oxide manometer for high-pressure magnetic resonance experiments, *Rev. Sci. Instrum.* **63**, 3120 (1992).
- [45] H. Fukazawa, N. Yamatoji, Y. Kohori, C. Terakura, N. Takeshita, Y. Tokura, and H. Takagi, Manometer extension for high pressure measurement: Nuclear quadrupole resonance study of Cu_2O with a modified Bridgman anvil cell up to 10 GPa, *Rev. Sci. Instrum.* **78**, 015106 (2007).
- [46] $1/T_1$ at each T is determined by fitting the nuclear magnetization M versus time t dependence after saturation using the exponential function $1 - M(t)/M(\infty) = \exp[-(t/T_1)^\beta]$. Here $M(t)$ and $M(\infty)$ are the nuclear magnetization at time t after saturation and the equilibrium nuclear magnetization at time $t \rightarrow \infty$, respectively. β was found to be unity in the normal state, and starts decreasing in the superconducting state, reaching ~ 0.7 at low temperatures. Different from the previous reports in which the recovery curves in T_1 measurement in $\text{FeTe}_{1-x}\text{Se}_x$ show non-single-exponential behavior [47–50], the recovery curves in this study show the single-exponential behavior in the normal state. See details in the Supplemental Materials [42].
- [47] D. Arčon, P. Jeglič, A. Zorko, A. Potočnik, A. Y. Ganin, Y. Takabayashi, M. J. Rosseinsky, and K. Prassides, Coexistence of localized and itinerant electronic states in the multiband iron-based superconductor $\text{FeSe}_{0.42}\text{Te}_{0.58}$, *Phys. Rev. B* **82**, 140508(R) (2012).
- [48] Y. Shimizu, T. Yamada, T. Takami, S. Niitaka, H. Takagi, and M. Itoh, Pressure-Induced Antiferromagnetic Fluctuations in the Pnictide Superconductor $\text{FeSe}_{0.5}\text{Te}_{0.5}$: ^{125}Te NMR Study, *J. Phys. Soc. Jpn.* **78**, 123709 (2009).
- [49] C. Michioka, H. Ohta, M. Matsui, J. Yang, K. Yoshimura, and M. Fang, Macroscopic physical properties and spin dynamics in the layered superconductor $\text{Fe}_{1+\delta}\text{Te}_{1-x}\text{Se}_x$, *Phys. Rev. B* **82**, 064506 (2010).
- [50] Y. Hara, H. Kotegawa, H. Nohara, H. Tou, Y. Mizuguchi, and Y. Takano, Se/Te-NMR study of $\text{Fe}(\text{Te}_{1-x}\text{Se}_x)$, *J. Phys. Soc. Jpn.* **80**, SA119 (2011).
- [51] T. Hanaguri, S. Niitaka, K. Kuroki, and H. Takagi, Unconventional s -wave superconductivity in $\text{Fe}(\text{Se},\text{Te})$, *Science* **328**, 474 (2010).
- [52] S. Sarkar, J. Van Dyke, P. O. Sprau, F. Massee, U. Welp, W.-K. Kwok, J. C. S. Davis, and D. K. Morr, Orbital superconductivity, defects, and pinned nematic fluctuations in the doped iron chalcogenide $\text{FeSe}_{0.45}\text{Te}_{0.55}$, *Phys. Rev. B* **96**, 060504(R) (2017).
- [53] S.-F. Wu, A. Almoalem, I. Feldman, A. Lee, A. Kanigel, and G. Blumberg, Superconductivity and Phonon Self-Energy Effects in $\text{Fe}_{1+y}\text{Te}_{0.6}\text{Se}_{0.4}$, *Phys. Rev. Res.* **2**, 013373 (2020).
- [54] A similar enhancement of $1/T_1$ of ^{125}Te under pressure has been reported in a powder form of $\text{FeSe}_{0.5}\text{Te}_{0.5}$ in Ref. [48].
- [55] K. Kitagawa, N. Katayama, K. Ohgushi, and M. Takigawa, Antiferromagnetism of SrFe_2As_2 Studied by Single-Crystal ^{75}As -NMR, *J. Phys. Soc. Jpn.* **78**, 063706 (2009).
- [56] S. Kitagawa, Y. Nakai, T. Iye, K. Ishida, Y. Kamihara, M. Hirano, and H. Hosono, Stripe antiferromagnetic correlations in $\text{LaFeAsO}_{1-x}\text{F}_x$ probed by ^{75}As NMR, *Phys. Rev. B* **81**, 212502 (2010).
- [57] M. Hirano, Y. Yamada, T. Saito, R. Nagashima, T. Konishi, T. Toriyama, Y. Ohta, H. Fukazawa, Y. Kohori, Y. Furukawa, K. Kihou, C.-H. Lee, A. Iyo, and H. Eisaki, Potential Antiferromagnetic Fluctuations in Hole-Doped Iron-Pnictide Superconductor $\text{Ba}_{1-x}\text{K}_x\text{Fe}_2\text{As}_2$ Studied by ^{75}As Nuclear Magnetic Resonance Measurement, *J. Phys. Soc. Jpn.* **81**, 054704 (2012).
- [58] Y. Furukawa, B. Roy, S. Ran, S. L. Bud'ko, and P. C. Canfield, Suppression of electron correlations in the collapsed tetragonal phase of CaFe_2As_2 under ambient pressure demonstrated by ^{75}As NMR/NQR measurements, *Phys. Rev. B* **89**, 121109(R) (2014).
- [59] A. Pandey, D. G. Quirinale, W. Jayasekara, A. Sapkota, M. G. Kim, R. S. Dhaka, Y. Lee, T. W. Heitmann, P. W. Stephens, V. Ogloblichev, A. Kreyssig, R. J. McQueeney, A. I. Goldman, A. Kaminski, B. N. Harmon, Y. Furukawa, and D. C. Johnston, Crystallographic, electronic, thermal, and magnetic properties of single-crystal SrCo_2As_2 , *Phys. Rev. B* **88**, 014526 (2013).
- [60] Q.-P. Ding, P. Wiecki, V. K. Anand, N. S. Sangeetha, Y. Lee, D. C. Johnston, and Y. Furukawa, Volovik effect and Fermi-liquid behavior in the s -wave superconductor CaPd_2As_2 : ^{75}As NMR-NQR measurements, *Phys. Rev. B* **93**, 140502(R) (2016).
- [61] Z. Xu, J. A. Schneeloch, J. Wen, E. S. Božin, G. E. Granroth, B. L. Winn, M. Feygenson, R. J. Birgeneau, G. Gu, I. A. Zaliznyak, J. M. Tranquada, and G. Xu,

- Thermal evolution of antiferromagnetic correlations and tetrahedral bond angles in superconducting $\text{FeTe}_{1-x}\text{Se}_x$, *Phys. Rev. B* **93**, 104517 (2016).
- [62] X. Wang, Y. Schattner, E. Berg, and R. M. Fernandes, Superconductivity mediated by quantum critical antiferromagnetic fluctuations: The rise and fall of hot spots, *Phys. Rev. B* **95**, 174520 (2017).
- [63] M. Toyoda, Y. Kobayashi, and M. Itoh, Nematic fluctuations in iron arsenides NaFeAs and LiFeAs probed by ^{75}As NMR, *Phys. Rev. B* **97**, 094515 (2018).
- [64] Y. M. Dai, H. Miao, L. Y. Xing, X. C. Wang, P. S. Wang, H. Xiao, T. Qian, P. Richard, X. G. Qiu, W. Yu, C. Q. Jin, Z. Wang, P. D. Johnson, C. C. Homes, and H. Ding, Spin-Fluctuation-Induced Non-Fermi-Liquid Behavior with Suppressed Superconductivity in $\text{LiFe}_{1-x}\text{Co}_x\text{As}$, *Phys. Rev. X* **5**, 031035 (2015).
- [65] J. Yang, R. Zhou, L.-L. Wei, H.-X. Yang, J.-Q. Li, Z.-X. Zhao, and G.-Q. Zheng, New Superconductivity Dome in $\text{LaFeAsO}_{1-x}\text{F}_x$ Accompanied by Structural Transition, *Chin. Phys. Lett.* **32**, 107401 (2015).
- [66] T. Kissikov, R. Sarkar, M. Lawson, B. T. Bush, E. I. Timmons, M. A. Tanatar, R. Prozorov, S. L. Bud'ko, P. C. Canfield, R. M. Fernandes, W. F. Goh, W. E. Pickett, and N. J. Curro, NMR study of nematic spin fluctuations in a detwinned single crystal of underdoped $\text{Ba}(\text{Fe}_{1-x}\text{Co}_x)_2\text{As}_2$, *Phys. Rev. B* **96**, 241108(R) (2017).
- [67] N. J. Curro, T. Kissikov, M. A. Tanatar, R. Prozorov, S. L. Bud'ko, and P. C. Canfield, Nematicity and Glassy Behavior Probed by Nuclear Magnetic Resonance in Iron-Based Superconductors, *Front. Phys.* **10**, 877628 (2022).
- [68] M. Toyoda, A. Ichikawa, Y. Kobayashi, M. Sato, and M. Itoh, In-plane anisotropy of the electric field gradient in $\text{Ba}(\text{Fe}_{1-x}\text{Co}_x)_2\text{As}_2$ observed by ^{75}As NMR, *Phys. Rev. B* **97**, 174507 (2018).
- [69] P. Malinowski, Q. Jiang, J. J. Sanchez, J. Mutch, Z. Liu, P. Went, J. Liu, P. J. Ryan, J. W. Kim, and J. H. Chu, Suppression of superconductivity by anisotropic strain near a nematic quantum critical point, *Nat. Phys.* **16**, 1189 (2020).
- [70] A. P. Dioguardi, T. Kissikov, C. H. Lin, K. R. Shirer, M. N. Lawson, H.-J. Grafe, J.-H. Chu, I. R. Fisher, R. M. Fernandes, and N. J. Curro, NMR Evidence for Inhomogeneous Nematic Fluctuations in $\text{BaFe}_2(\text{As}_{1-x}\text{P}_x)_2$, *Phys. Rev. Lett.* **116**, 107202 (2016).
- [71] C. Eckberg, D. J. Campbell, T. Metz, J. Collini, H. Hodovanets, T. Drye, P. Zavalij, M. H. Christensen, R. M. Fernandes, S. Lee, P. Abbamonte, J. W. Lynn, and J. Paglione, Sixfold enhancement of superconductivity in a tunable electronic nematic system, *Nat. Phys.* **16**, 346 (2020).
- [72] P. S. Wang, P. Zhou, S. S. Sun, Y. Cui, T. R. Li, H. Lei, Z. Wang, and W. Yu, Robust short-range-ordered nematicity in FeSe evidenced by high-pressure NMR, *Phys. Rev. B* **96**, 094528 (2017).
- [73] C. Wuttke, F. Caglieris, S. Sykora, F. Steckel, X. Hong, S. Ran, S. Khim, R. Kappenberger, S. L. Bud'ko, P. C. Canfield, S. Wurmehl, S. Aswartham, B. Büechner, and C. Hess, Ubiquitous enhancement of nematic fluctuations across the phase diagram of iron based superconductors probed by the Nernst effect, *npj Quantum Mater.* **7**, 82 (2022).